Research Article

Yuqing Peng, Zhiwei Li, Aijun Li, Qifan Wang, Ruicheng Bai and Fangzhou Zhang*

Mechanical and tribological properties of C/C–SiC ceramic composites with different preforms

https://doi.org/10.1515/secm-2022-0205
received January 01, 2023; accepted April 24, 2023

Abstract: The C/C–SiC composites were fabricated by the liquid silicon infiltration method. The mechanical and tribological properties of C/C–SiC composites were assessed and compared based on different C/C densities and the carbon fiber textile architecture. The results demonstrated that the bending and shear strengths of C/C–SiC were lower than those of C/C composites, which resulted from the carbon fibers being corroded during the process of infiltration of liquid silicon. In contrast to C/C composites, the compressive strength of C/C–SiC exhibited higher values due to the presence of SiC ceramics. Moreover, the mechanical strength of C/C composites increased gradually with the increase of the C/C preform density. The tribological properties of various C/C–SiC composites showed a stable friction phase at an intermediate braking stage. When the density of C/C preforms was around 1.78 g/cm^3, the C/C–SiC composites exhibited excellent friction coefficients (0.438 and 0.465), and low wear rates (linear and weight wear rates were 0.450 μm/time and 0.123 g/cycle, respectively). Furthermore, the C/C–SiC composites fabricated with non-woven carbon fiber needling preforms showed relatively a higher friction value and wear rate than those of C/C–SiC with PANOF integral C/C preforms. Therefore, C/C–SiC composites have been considered promising friction materials for braking system applications.

* **Corresponding author: Fangzhou Zhang,** Institue of Materials, Shanghai University, 200072 Shanghai, China; Shaoxing Institute of Technology, Shanghai University, Shanghai 200072, China, e-mail: zhangfzh@shu.edu.cn
Yuqing Peng, Zhiwei Li, Qifan Wang: Institue of Materials, Shanghai University, 200072 Shanghai, China
Aijun Li: Institue of Materials, Shanghai University, 200072 Shanghai, China; Shaoxing Institute of Technology, Shanghai University, Shanghai 200072, China
Ruicheng Bai: Research Center for Composite Materials, Shanghai University, 20044 Shanghai, China

Keywords: C/C–SiC, tribological properties, liquid silicon infiltration, chemical vapor infiltration, fiber architecture

1 Introduction

Carbon/carbon (C/C) composites exhibit low density, high thermal conductivity, good shock resistance, low thermal expansion, high modulus, and good wear properties [1]. Owing to these excellent properties, they are used as friction pads or rings for braking material systems [1,2]. However, active oxidation behavior is seen in C/C composites at temperatures above 400°C; meanwhile, in combination with the instability of the coefficient of friction (COF) caused by humidity and temperature, it leads to material failure and limits their service life [3,4]. Carbon fiber-reinforced carbon–silicon carbide matrix (C/C–SiC) composites have been initially developed in order to enhance the oxidation resistance of C/C composites because SiC ceramics exhibit improved oxidation protection for C/C composites. Furthermore, the addition of SiC to C/C composites not only retains the advantages of C/C composites but also shows some superior properties, such as better oxidation resistance, high thermal shock resistance, and longer service life, especially lower sensitivity to surroundings and temperature [5–10]. Therefore, C/C–SiC composites have been considered promising candidates for brake discs or pad applications.

The C/C–SiC composites are commonly fabricated by the liquid silicon infiltration (LSI) process, in which molten silicon impregnates porous carbon/carbon composites and reacts with the carbon to form silicon carbide [11]. As the porous C/C composite is a source for the preparation of C/C–SiC composites by using the LSI process, thus, the architecture of the properties of C/C–SiC composites are highly dependent on the composition and structure of porous C/C composites. However, a few studies concerning the effect of these factors (i.e., density, porosity. and the architecture structure) on mechanical

and tribological properties have been reported, and consequently, only scarce information is available in the literature [12]. Zhang et al. [13] fabricated C/C–SiC composites by using four kinds of needled C/C preforms with the same fiber volume fraction and different pyrocarbon contents. They found that the residual pyrocarbon content in the C/C preforms has a great influence on the properties of C/C–SiC composites; the flexural strength and shear strength of the composites tend to gradually increase as the amount of the residual pyrocarbon increases [13]. Meanwhile, they also found that the frictional properties can be effectively controlled by the composition and the phase content (SiC, Si, and pyrocarbon) [14]. Zhou et al. have investigated the effect of the porosity of C/C preforms and SiC contents on the tribological properties of C/C–SiC composites that are fabricated by hybrid technology. The friction coefficient increases, while the braking time and wear rate decrease as the original preform density increases. This difference has been demonstrated and is attributed to the effect of the SiC content and porosity.

In the present work, the porous C/C composites with different densities were prepared by hybrid technology (chemical vapor infiltration and polymer infiltration pyrolysis), followed by the LSI process to fabricate C/C–SiC composites. Additionally, the effects of the density of the porous C/C composites and the architecture structure of carbon fiber preforms on the mechanical and tribological properties of C/C–SiC composites were evaluated.

2 Experimental procedures

2.1 Preparation of C/C–SiC composites

C/C–SiC composites were fabricated from porous C/C composites by the LSI process in two steps: preparing the porous C/C composite and subsequently the C/C–SiC composite. First, C/C composites were prepared by chemical vapor infiltration using carbon preforms with different architectures. One is the non-woven needled carbon felt, as shown in Figure 1a; the other is the PAN-based integral felt (PANOF), as shown in Figure 1b. Then, C/C–SiC composites were fabricated by the LSI method. The fabrication process of C/C porous composites and C/C–SiC composites are shown in Figure 2. The properties of the C/C and C/C–SiC composites are listed in Table 1, which are labeled using different capital letters. The C/C composites with a high density (ca. 1.88 g/cm^3, sample D) were fabricated by hybrid methods for comparison.

2.2 Characterization

The open porosity and bulk density of the samples were determined by the Archimedes method. The X-ray diffraction (XRD) patterns of the C/C–SiC composites were recorded using an XRD (DLMAX-2550, Rigaku, Japan)

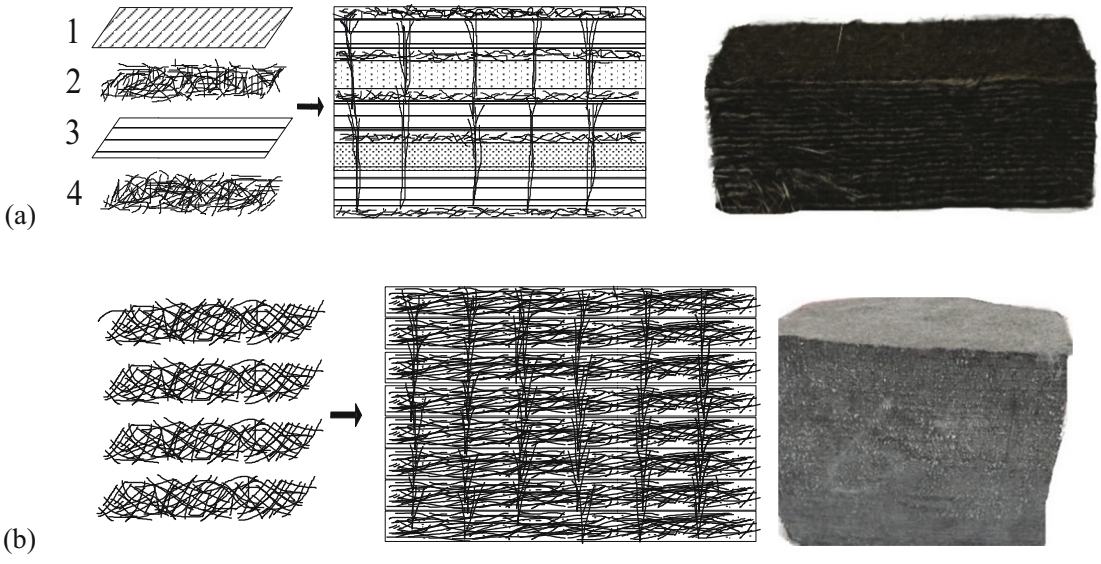

Figure 1: Schematic diagram of non-woven fiber cloth carbon preforms (a) (1: 0° non-woven fiber cloth; 2, 4: short-cut fiber web; 3: 90° non-woven fiber cloth) and PANOF integrated felt (b).

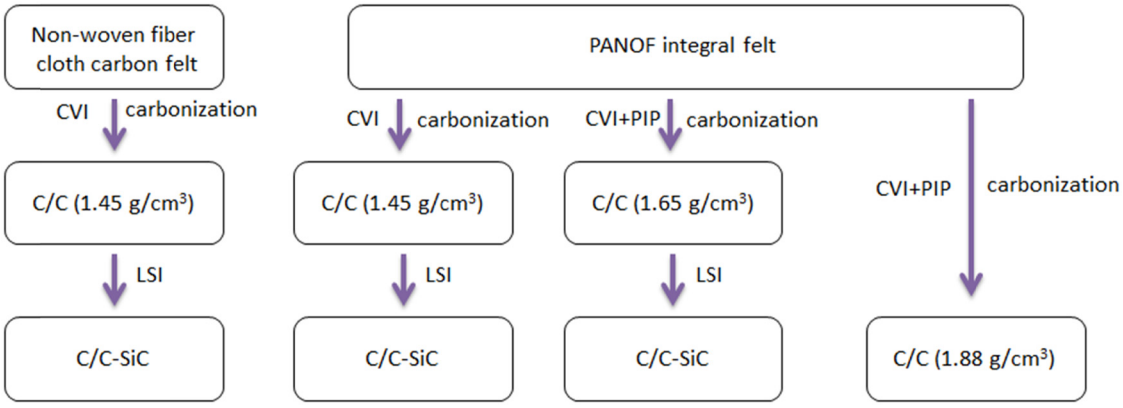

Figure 2: Schematic flow chart illustrating the preparation of C/C–SiC composites with different densities derived from porous C/C composites.

Table 1: Properties of as-obtained C/C and C/C–SiC composites

Sample	Architecture structure of porous C/C composites	C/C composites		C/C–SiC composites	
		Density (g/cm³)	Porosity (%)	Density (g/cm³)	Porosity (%)
A	PANOF integral felt	1.44	28.75	2.20	4.46
B		1.53	23.15	1.98	6.82 (4.82)
C		1.65	13.82	1.98	7.75 (4.85)
G		1.78	7.03	1.93	2.94
D		1.88	3.51	—	—
E	Non-woven needled carbon felt	1.45	26.33	1.99	13.87

Note: Samples A–E are used for characterization of mechanical properties, while samples A, C, G, D, and E are used for frictional and wear experiments.

equipped with monochromatic Cu Kα radiation in a reflection mode. The scan step size was 0.05° in the reflection range of 10–80°. The surface and fracture microstructures were observed using a scanning electron microscope (SEM; HITACHI SU-1500, HITACHI, Japan).

The mechanical properties of C/C–SiC composites were evaluated under bending, shearing, and compressive conditions. The bending strength and shear strength of the samples with dimensions 35 mm × 4 mm × 3 mm were determined using three-point bending with a span of 30 mm, while the samples with dimensions 10 mm × 10 mm × 10 mm were used for determining the compressive strength; they were measured on an MTS-CMT-4204. The equations of bending (σ_f), shearing (τ), and compressive strength (σ_c) are presented as follows in equations (1)–(3), respectively:

$$\sigma_f = \frac{3FL}{2bh^2}, \tag{1}$$

$$\tau = \frac{3F}{4bh}, \tag{2}$$

$$\sigma_c = \frac{F}{S}, \tag{3}$$

where F and L are the loading and the length of the support span, respectively, b and h represent the width and thickness of the samples, respectively, and S denotes the contact surface area of the samples during compression testing.

The tribological properties of C/C–SiC brake materials were tested on an MM1000-II999 disk-on-disk type laboratory scale dynamometer test rig (Figure 3). Both stators and rotors (i.e., counterpart) used for friction testing are C/C–SiC specimens. The size of rotor specimens is Φ 76–52 × 10 mm (76 mm in outer diameter, 52 mm in inner diameter, and 10 mm in thickness), while that of stator specimens is Φ 89–79 × 10 mm (Figure 4). The brake speed, brake pressure, and brake moment were designed at 6,340 rpm, 1.04 MPa, and 0.1 kg m^2, respectively. During the experiment, the rotating velocity, brake moment, and brake time were simultaneously recorded. The thickness and mass of the rotating disc and the stationary disc were measured before and after braking

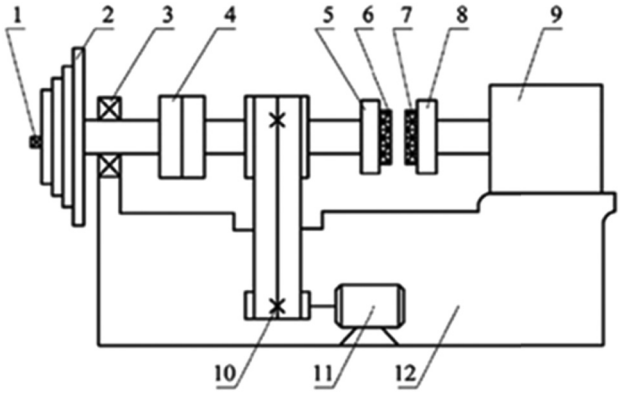

Figure 3: Schematic diagram of the tribological testing machine: (1) clamp nut, (2) inertial wheel, (3) bearing, (4) clutch, (5) rotor holder, (6) rotor, (7) stator, (8) stator holder, (9) pressing cylinder, (10) strap, (11) motor, and (12) lathe bed.

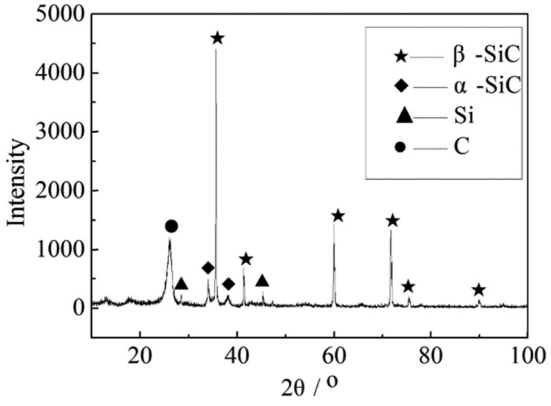

Figure 5: XRD patterns of the as-received C/C–SiC composites.

tests, giving the corresponding linear and weight wear rates, respectively. The aforementioned experimental tests were repeated 20 times to obtain average values. The coefficient friction (μ) was calculated according to the following equation:

$$\mu = \frac{M}{P \cdot R},$$

where M is the braking torch, and P and R are the brake pressure and mean radius, respectively.

3 Results and discussion

3.1 Phase analysis of C/C–SiC composites

The use of advanced characterization techniques such as XRD helps to identify the type of phases and their location in the microstructure [15]. The phase analysis of C/C–SiC composites determined by XRD showed the presence of silicon carbide, carbon, and unreacted silicon phases (Figure 5). The face-centered cubic (β) polytype is the main phase of silicon carbide. The carbon peak is assigned to the carbon fibers and unreacted pyrocarbon. The optical metallographic photos of C/C–SiC composites (Figure 6) showed that the pyrolytic carbon in the CVI carbon matrix was found around the carbon fibers (Figure 6(b)), while the resin carbon was far away from the carbon fibers (Figure 6(a)). A large number of β-SiC grains forming from the siliconizing reaction of liquid silicon and pyrolytic carbon can be observed around the pyrocarbon and resin carbon (Figure 6(a)); thus, the residual silicon was wrapped by the SiC phase. Additionally, regularly spaced segmentation cracks, micro-delamination, could be observed in C/C composites (Figure 6(c)) [15]. Moreover, these cracks seem to provide a channel for the infiltration of liquid silicon; after an initial reaction between the carbon and silicon vapor, liquid silicon needs to penetrate the already formed SiC layer so that the growth

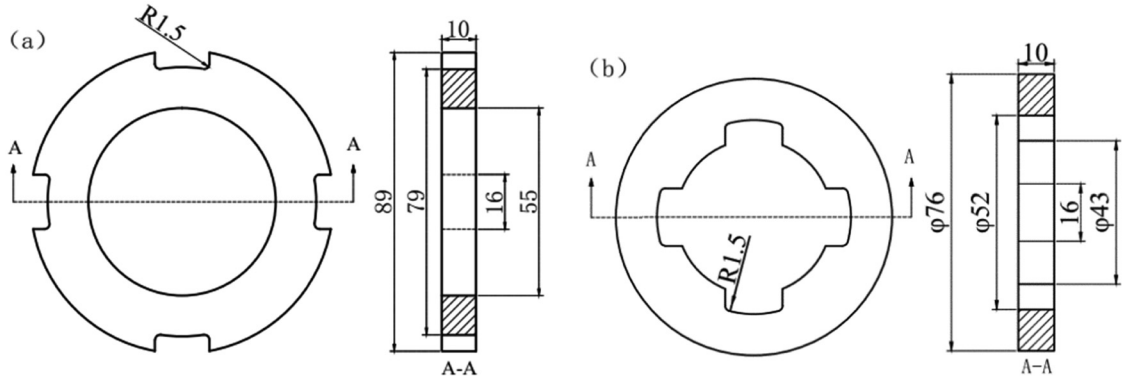

Figure 4: Schematic diagram of the testing specimen and counterpart: (a) stator specimen and (b) rotor specimen.

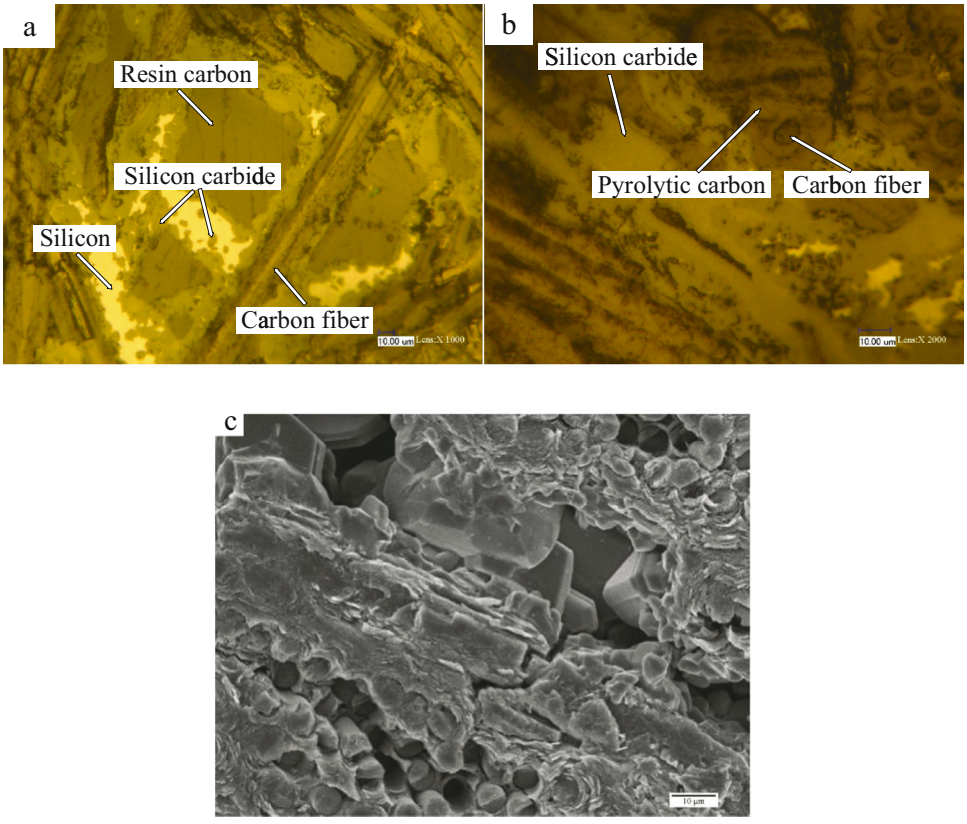

Figure 6: The structure image of C/C–SiC composites: (a) and (b) metallographic photos and (c) microstructure image of C/C–SiC composites.

of the SiC layer is controlled by the diffusion of silicon. Thus, β-SiC grains stacked in the crack or micro-delamination sites were observed. Furthermore, a violent reaction and a high number of nucleation sites led to the formation of a fine-grained SiC with a high density of stacking faults, which is consistent with the findings in previous work [16].

It is noted that highly localized, exothermic reaction in combination with reduced heat conductivity causes a local peak temperature (>2,000°C), which is high enough to promote the β → α transformation [17,18]. Thus, the peak diffraction corresponding to α-SiC was also found in our prepared C/C–SiC composites.

3.2 Mechanical properties of C/C–SiC composites

The mechanical properties (i.e., bending, shear, and compressive strength) of C/C–SiC composites (samples A–C and E) are listed in Table 2, compared to C/C composites with high density (sample D). It was found that C/C–SiC composites showed lower values of flexural strength and shear strength after impregnation of silicon than those of C/C composites with a high densification degree (sample D). The decrease in the composite strength was probably related to the carbon fibers being corroded by liquid silicon. Interestingly, the compressive strength of C/C–SiC composites exhibits higher values compared to that of C/C composites, which was probably related to the formation of the SiC ceramics matrix.

By comparing samples A, B, and C, it was found that the mechanical properties of the C/C–SiC increased with

Table 2: Mechanical properties of C/C–SiC composites

Sample	Bending strength		Shear strength		Compressive strength	
	XY	*Z*	*XY*	*Z*	*XY*	*Z*
A	62.1	24.8	15	7.5	180	138
B	70	30	20	8.5	190	150
C	75	33	22.5	9	240	180
D	90	45	27.5	15	178	160
E	200	180	45	38	200	—

the increase of density of the porous C/C from PANOF preforms. As the original C/C preform with high porosity could provide more space for infiltration of liquid silicon, a large amount of silicon was filled in the porous C/C preforms with high open porosity during the LSI process, leading to the formation of silicon carbide and excess silicon. Meanwhile, due to the reaction of excess silicon with carbon fibers, the strength of the C/C–SiC composite decreased. Consequently, with a decrease in the density and a corresponding increase in the porosity of the porous C/C, the C/C–SiC composite prepared by LSI presents a lower strength. Therefore, the mechanical properties of sample A with the highest density of C/C showed the lowest values.

Furthermore, the composites loaded in the *XY* direction exhibited higher strength values than those in the *Z* direction, which is attributed to a higher volume fraction of carbon fibers in the *XY* direction (Table 2). The flexural morphologies of C/C–SiC composites are presented in Figure 7; a higher amount of fibers' pull-out was observed in the fracture surface of the sample from the *XY* direction as compared to that of the *Z* direction.

The corresponding stress–strain curves and morphologies are shown in Figure 8. Sample A showed brittle fracture behavior, whereas samples C and D presented ductile fracture behavior. This was consistent with the SEM image: a uniform fracture surface was observed in sample A, while a fiber pull-out was clearly visible in

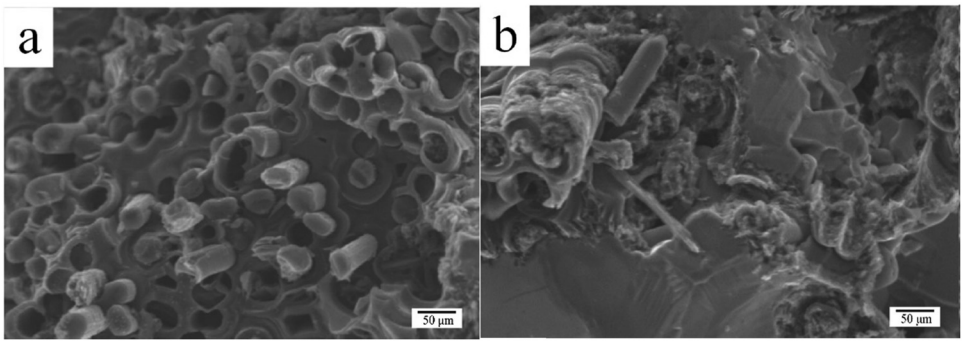

Figure 7: Flexural morphologies of C/C–SiC composites. Sample A: (a) *XY* direction and (b) *Z* direction.

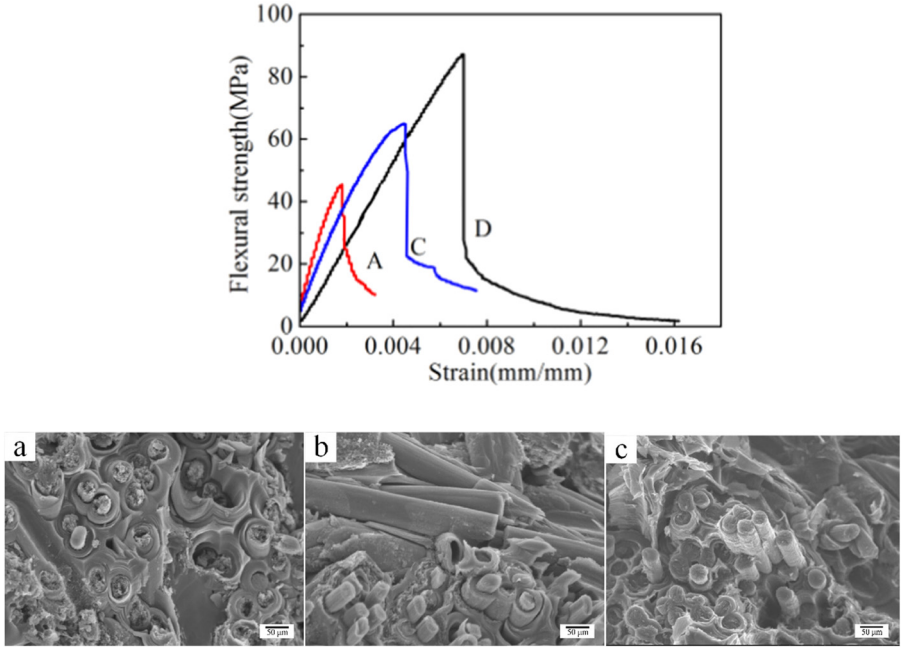

Figure 8: Flexural stress–strain curves and morphologies of samples: (a) sample A, (b) sample C, and (c) sample D.

samples C and D. For sample A, due to the strong chemical bonding between the SiC matrix and the pyrocarbon/carbon fibers in the composite, the crack formed within the SiC matrix could not be propagated and deflected. In contrast, the weak interface cohesion between the pyrolytic carbon and the carbon fibers in C/C composites was beneficial to transfer the loadings and deflecting the crack around the carbon fibers, resulting in the fiber pull-out in C/C composites.

Additionally, the effect of the carbon fiber preform architecture on the mechanical properties of C/C–SiC is also discussed. The stress–strain curves of C/C composites with different carbon fiber architectures are presented in Figure 9. The C/C–SiC composites fabricated with non-woven fiber cloth needled porous C/C (sample E) showed higher strength than that of the PANOF integral C/C (sample A). Moreover, from the flexural stress–-strain curve, sample A presented typical brittle fracture behavior (Figures 9 and 10), while sample E exhibited typical non-brittle fracture behavior. Furthermore, the shear and compressive stress–strain curve of sample E showed an indication of pseudoplastic behavior. In the compressive stress–strain curve, the stress loading as a function of the strain of sample A followed a linear relationship and then suddenly decreased, whereas a non-linear behavior occurring at the initial loading increased linearly, and then the load gradually decreased after reaching the peak of load. The higher values of strength for sample E probably contributed to a higher carbon fiber content in the resultant C/C–SiC composites (Figure 10). As can be seen in Figure 10, the carbon fibers in sample E were distributed more homogenously and stacked as compared to that in sample A. Thus, the higher load can be transferred in sample E due to the higher carbon fiber content, which led to crack propagation and further increased the displacement.

Furthermore, the optical photographs of the fracture surfaces obtained from flexural loading are shown in Figure 11. It shows that the fracture surface of sample A was flat and uniform, whereas the typical fiber pull-out was clearly visible in sample E, which can also confirm the ductility behavior.

4 Friction and wear properties of C/C–SiC composites

The friction and wear properties of C/C–SiC were tested using a full-size aircraft wheel and brake assembly on a

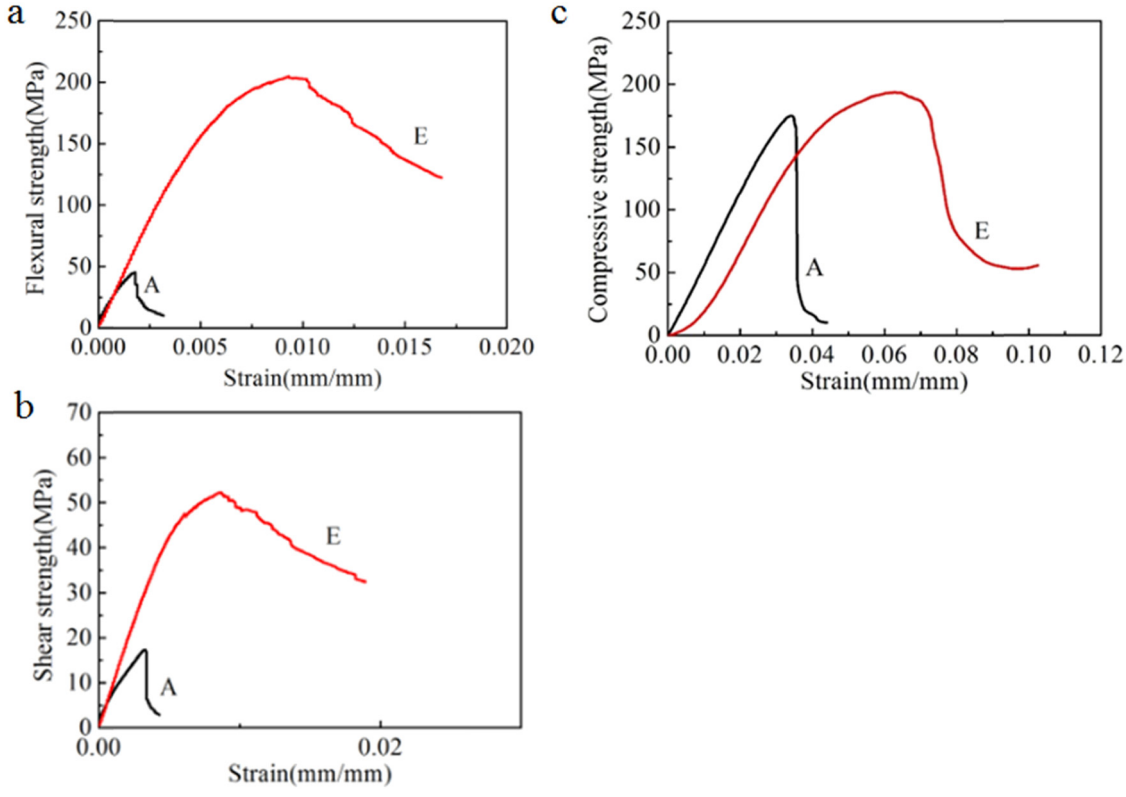

Figure 9: The various composite stress–strain curves with different porous C/C composite architecture structures: (a) flexural stress–strain curves, (b) shear stress–strain curves, and (c) compressive stress–strain curves.

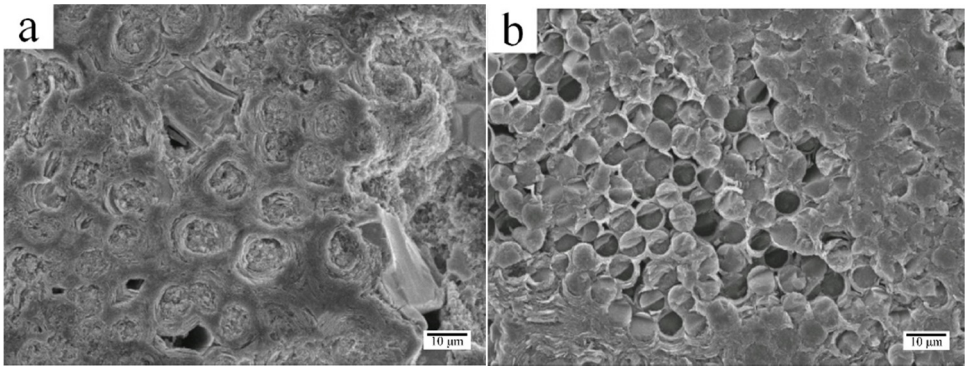

Figure 10: The morphology of samples with different porous C/C composite architecture structures: (a) sample A and (b) sample E.

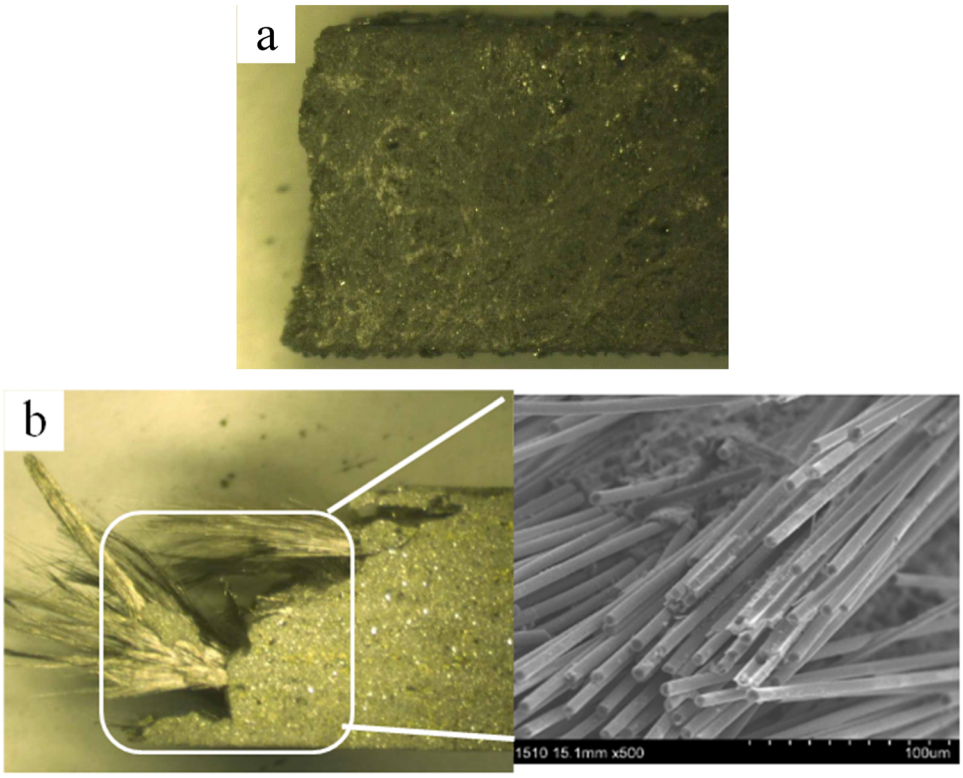

Figure 11: Typical optical macrographs and SEM morphology of the fractured C/C–SiC composites upon flexural loading test: (a) sample A and (b) sample E.

full-scale dynamometer. The COF (μ) of C/C–SiC discs during the braking tests are shown in Figure 12. The friction and wear properties of samples A, C, G, D, and E are listed in Table 3.

Figure 12 shows all COF curves that present a typical saddle shape: a "pre-peak" at the initial stage of braking and a rapidly increasing stage, a "tail peak" at the end of braking; sample D did not show the phenomenon of "tail peak" at the end of braking. Initially, the braking started with a decrease in the speed, and the rough grains of the sample surface were embedded mutually and generated new abrasive particles due to the effect of the surface pressure of the brake pairs. Thus, the sudden increase of the COF would be observed in all samples. With the progress of friction, the debris on the surface of the sample was rolled into a friction film, the friction film could play a certain role of lubrication, so that the friction force was reduced, with the stability of the friction pressure, the dynamic friction coefficient presented a stable feature, as shown in the intermediate section of these curves. At the end of braking, the

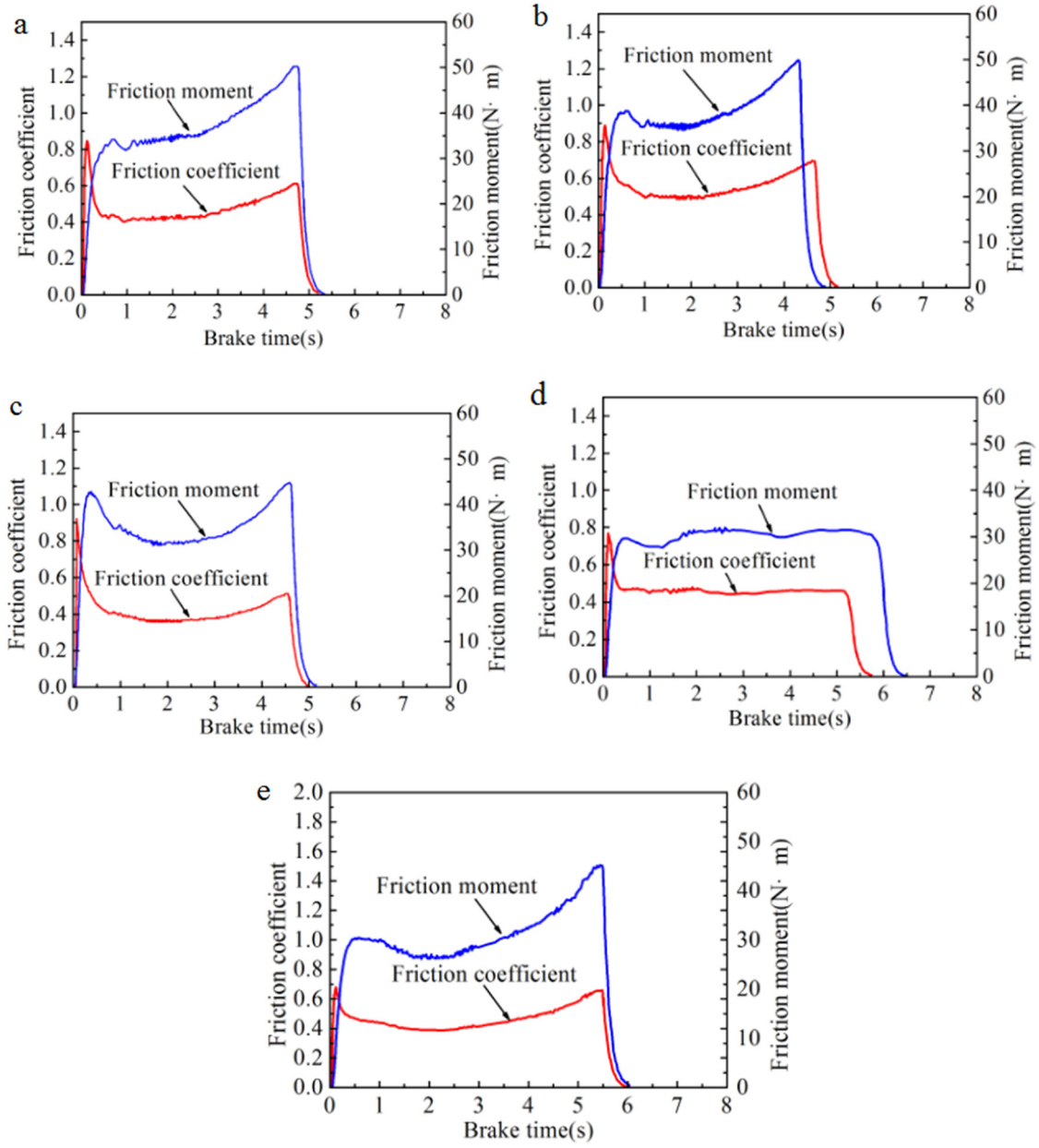

Figure 12: Braking curve of the friction coefficient and moment for samples A, C, G, and D, E. (a) Sample A, (b) Sample C, (c) Sample G, (d) Sample D, and (e) Sample E.

Table 3: Friction and wear properties of samples A, C, G, D, and E

Sample	Average torque (N m)	Maximum torque (N m)	Torque stability coefficient (%)	Friction factor	Static friction coefficient	Linear wear rate (μm/time)	Weight wear rate (g/cycle)	Brake time (s)	Absorbing power per unit area (W/cm^2)
A	37.233	50.547	73.700	0.462	0.495	0.600	0.131	4.434	541.823
C	39.578	50.286	78.773	0.575	0.611	1.588	0.402	4.214	575.947
G	34.657	42.475	81.414	0.438	0.465	0.450	0.123	4.860	504.348
D	33.231	38.482	87.291	0.425	0.447	0.400	0.111	5.130	483.582
E	33.595	48.292	69.690	0.465	0.614	0.687	0.227	5.065	488.883

high temperature caused by friction could lead to the decomposition of the material and structural flaw; thus, the COF increased in the final stage, which is commonly called the "rise of the tail" phenomenon in the COF curves [19].

Comparing C/C–SiC (samples A, C and G, see Figure 12a–c, respectively) and C/C composites (sample D, see Figure 12d), it was observed that the introduction of rigid SiC could generate new abrasive particles, which led to the increase in the surface roughness. Thus, the sharper "first peak" of C/C–SiC composites was observed in the COF curves as compared to that of C/C composites (sample D). With the increase of the braking time, the formation of the lubricant film resulted in constant COF values for all samples. Furthermore, it is known that the presence of SiC and Si in the composite matrix led to a higher friction coefficient [20], thus samples A, C, and G showed higher COF values (Table 3).

The effect of the density of C/C preforms on friction characteristics of C/C–SiC composites was intriguing. With a decrease in the density of the C/C preforms (samples A, C, and G), the content of silicon carbide and silicon that infiltrated into C/C preforms increased, which could increase COF values of C/C–SiC composites [14]. Thus, the rigid SiC phase works as a framework in the samples to enhance the friction, leading to higher average friction values (as shown in sample C). However, sufficient amounts of SiC or SiC particles with a small grain size might be pulverized as a layer of the frictional film with the braking process, which plays the role of lubricant, and thus the reduced friction coefficient can be found in sample A as compared to sample C. Additionally, studies have reported that graphite plays the role of a lubricant, and a suitable amount of graphite is helpful to form a friction film to reduce the wear rate; therefore, the friction films were formed on the surface and increased with the pyrolytic carbon content [21,22]. Thus, the higher the residual pyrolytic carbon, the lower the COF values, as shown in sample G as compared to sample C. Sample A exhibited a lower friction coefficient and wear rate than those in sample C, which was probably due to the presence of enough SiC in sample A, which easily formed a SiC lubricant film during friction testing.

For different fiber preform structures (samples A and E), the friction torque of sample E fluctuated greatly in the early stage and increased sharply in the later stage, as shown in Figure 12e. The tribological performance of sample A was better than that of sample E. The stability of the friction torque of sample E was low, vibration occurred in the friction process, and the process was unstable. The specific reasons can be observed from the friction and wear morphology analysis.

The friction and wear properties can be explained by studying the morphology [23]. The wear-induced surface microstructures of the C/C–SiC discs were investigated by SEM, as shown in Figure 13.

The surface of sample A was found to be the most flat (Figure 13a). This is because the SiC content of sample A was the highest and distributed continuously and evenly. Therefore, during the friction process, SiC was the main bearing phase and formed a lot of friction chips. It also filled around the SiC micro-convex body and these friction chips unshed formed the friction film, which is the main cause to enhance the tribological properties; this phenomenon belongs to adhesive wear. In contrast, the scratch surface was found in sample C after friction testing (Figure 13b), which was because the SiC content in sample C was intermediate and mainly existed in the form of large particles; it was easy to fall off and form large abrasive particles during the friction process. In terms of friction and wear performance, the friction coefficient and wear rate were the highest. The surface of sample G presented no scratches and formed a discontinuous friction film; this was because the SiC content in sample G was the least and existed in the form of small particles. So, in the process of friction, these small SiC particles quickly formed a friction film with other grinding chips; the friction coefficient was the smallest but because of the existence of hard SiC small particles, its wear rate was still higher than that of pure C/C composites (sample D). The friction surface of sample D was rough, the fiber morphology was clearly visible, and a complete friction film was not formed. Therefore, the friction coefficient was slightly higher than that in sample G but the wear rate was the lowest due to the graphite carbon lubrication.

The effect of different preform structures (samples A and E) on the morphology was compared. From Figure 13e, it can be observed that cracks and scratches caused by grinding particles are distributed on the surface of sample E after the friction test; the trace of the peeling fiber parallel to the *XY* direction is seen in Figure 13e. This is because the preform of sample E was non-woven needled carbon felt, so the content of fiber was more in the *XY* direction and was closely arranged. The content of pyrolytic carbon among fibers was less. The interface bond between the carbon fiber and pyrolytic carbon was weak and it was easy to flake off. The carbon fiber preform structure was easily damaged because the carbon fiber was eroded by fused Si, which resulted in serious surface wear of the sample. In addition, when the axial fiber distribution was small, the axial thermal conductivity was low, the surface heat dissipation of the sample was

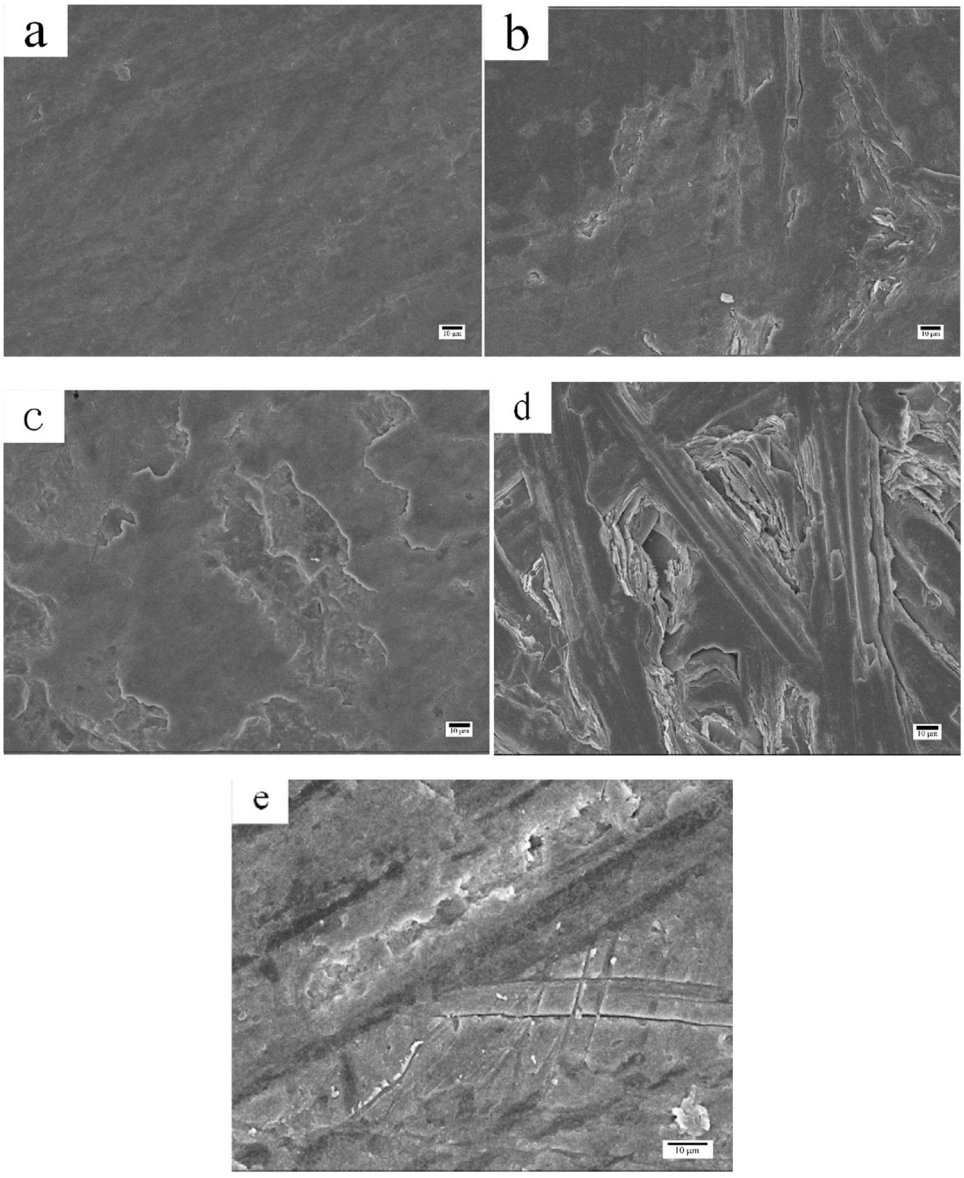

Figure 13: The surface micro-morphology of samples after friction testing ((a–e) correspond to samples A, C, G, D, and E, respectively).

slow, and it was easy to produce a high temperature. The molten Si caused by high temperatures easily adhered to the mating plate; meanwhile, the molten substances were pulled out by the shear stress, creating a hole on the surface, as shown in Figure 13e. Therefore, higher wear rates were seen in C/C–SiC composites with non-woven needled C/C preforms (sample E, Table 3).

Comparing the analysis of friction and wear properties of C/C–SiC composites with the same C/C porous composite density and different carbon fiber preform structures, it was found that the friction coefficient of C/C–SiC composites with PANOF integral felt was moderate, the friction process was more stable, the braking time was shorter, the wear rate was lower, and the overall tribological performances were better, as well as the main wear mechanisms were abrasive.

In this article, the friction and wear properties of C/C–SiC composites have been studied. In the future, the friction and wear properties of C/C–SiC composites shall be studied in the real application environment, for example, automobile brake discs. In addition, new fabrication methods of C/C–SiC brake discs could be adopted to reduce the influence of residual silicon, shorten the preparation cycle, and reduce the cost.

5 Conclusion

1) The determined mechanical strength (i.e., bending, shear, compressive strength) of C/C–SiC composites are proportional to the density of porous C/C preforms. Furthermore, the bending and shear strengths of C/C–SiC materials were shown to be lower than those of C/C composites, which are attributed to the degraded strength of carbon fibers during LSI processing. In contrast, the compressive strength between C/C–SiC and C/C composites in *XY* and *Z* directions showed that higher values were found in loading with *XY* directions in C/C–SiC composites and *vice versa* with the *Z* direction.
2) The effect of architecture structures on the mechanical properties indicated the C/C–SiC composites fabricated with non-woven carbon fibers needling C/C preforms posed superior mechanical properties than those of PANOF integral felt structures. Moreover, the latter showed pseudoplastic and ductile behavior, while the former showed a brittle fracture.
3) The friction coefficient curve of C/C–SiC composites exhibits a typical tribological behavior, showing a "pre-peak" at the initial stage of braking and a rapidly increasing stage "tail peak" at the end of braking. Furthermore, the friction properties are strongly dependent on the density of C/C preforms. The average friction factor of C/C–SiC composites first increases and then decreases with the increase in the density of C/C preforms. When the density of C/C preforms is around 1.78 g/cm^3, the resulting C/C–SiC composites show high friction coefficients (0.438 and 0.465), and low wear rates (linear and weight wear rates are 0.450 μm/time and 0.123 g/cycle, respectively). Additionally, the C/C–SiC composites fabricated with non-woven carbon fiber needling C/C preforms show relatively higher friction values and wear rates as compared to those of PANOF integral C/C preforms.

Acknowledgements: YQ Peng acknowledges the financial support from the National Natural Science Foundation of China (21676163, 51602189), Natural Science Foundation of Shanghai (18ZR1417700, 20ZR1419600), and Science and Technology on Advanced Functional Composites Laboratory Funding (6142906200110). The authors would also like to acknowledge Mr. Bo Li for his valuable contribution.

Conflict of interest: Authors state no conflict of interest.

Data availability statement: The raw/processed data required to reproduce these findings cannot be shared at this time as the data also forms part of ongoing study.

References

[1] Windhorst T, Blount G. Carbon-carbon composites: a summary of recent developments and applications. Mater Des. 1997;18(1):11–5.
[2] Li C, Crosky A. The effect of carbon fabric treatment on delamination of 2D-C/C composites. Compos Sci Technol. 2006;66(15):2633–8.
[3] Westwood ME, Webster JD, Day RJ, Hayes FH, Taylor R. Oxidation protection for carbon fibre composites. J Mater Sci. 1996;31(6):1389–97.
[4] Zhang J, Xu Y, Zhang L, Cheng L. Effect of Braking Speed on Friction and Wear Behaviors of C/C-SiC Composites. Int J Appl Ceram Technol. 2007;4(5):463–9.
[5] Zhang C, Zhou Y, Liu HR, Li JP, Lu KF, Li Y. Influence of pyrolytic carbon interphase and pyrolysis temperature on the mechanical and tribological properties of Cf/SiC after heat treatment at 1800°C. Ceram Int. 2021;47:16282–93.
[6] Xie J, Li K, Li H, Fu Q, Guo L. Ablation behavior and mechanism of C/C–ZrC–SiC composites under an oxyacetylene torch at 3000°C. Ceram Int. 2013;39(4):4171–8.
[7] Krenkel W, Berndt F. C/C–SiC composites for space applications and advanced friction systems. Mater Sci Eng: A. 2005;412(1–2):177–81.
[8] Krenkel W, Heidenreich B, Renz R. C/C-SiC Composites for Advanced Friction Systems. Adv Eng Mater. 2002;4(7):427–36.
[9] Li Z, Liu YZ, Zhang BG, Lu YH, Li Y, Xiao P. Microstructure and tribological characteristics of needled C/C–SiC brake composites fabricated by simultaneous infiltration of molten Si and Cu. Tribol Int. 2016;93(Part A):220–8.
[10] Zhang C, Liu H, Zhou Y, Li J, Sun Y, Wang Y, et al. The effect of high temperature heat treatment on the tribological property of a carbon fiber/pyrolytic carbon/silicon carbide composite using polycarbosilane. Ceram Int. 2020;46:4493–4501.
[11] Fitzer E, Gadow R. Fiber-reinforced silicon carbide. Am Ceram Soc Bull. 1986;65(2):326–35.
[12] Wang H, Zhu D, Wan F, Zhou W, Luo F. Influence of the C/C preform density on tribological characteristics of C/C–SiC composites under different conditions. Ceram Int. 2014;40(10, Part B):16641–6.
[13] Zhang Y, Xiao Z, Wang J, Yang J, Jin Z. Effect of pyrocarbon content in C/C preforms on microstructure and mechanical properties of the C/C–SiC composites. Mater Sci Eng: A. 2009;502(1–2):64–9.
[14] Zhang YH, Xiao ZC, Wang JP, Xing RP, Peng ZG, Su JM, et al. Effect of pyrocarbon content on thermal and frictional properties in C/C preforms of C/C–SiC composites. Wear. 2010;269(1–2):132–8.
[15] Akhtar1 M, Khajuria K, Sahu KJ, Swaminathan J, Kumar R, Bedi R, et al. Phase transformations and numerical modelling in simulated HAZ of nanostructured P91B steel for

high temperature applications. Appl Nanosci. 2018;8(7):1669–85.
[16] Schulte-Fischedick J, Zern A, Mayer J, Rühle M, Frieß M, Krenkel W, et al. The morphology of silicon carbide in C/C–SiC composites. Mater Sci Eng: A. 2002;332(1–2):146–52.
[17] Sawyer GR, Page TF. Microstructural characterization of "REFEL" (reaction-bonded) silicon carbides. J Mater Sci. 1978;13(4):885–904.
[18] Ness JN, Page TF. Microstructural evolution in reaction-bonded silicon carbide. J Mater Sci. 1986;21(4):1377–97.
[19] Zhou X, Zhu D, Xie Q, Luo F, Zhou W. Friction and wear properties of C/C–SiC braking composites. Ceram Int. 2012;38(3):2467–73.
[20] Fouquet S, Rollin M, Pailler R, Bourrat X. Tribological behaviour of composites made of carbon fibres and ceramic matrix in the Si–C system. Wear. 2008;264(9–10):850–6.
[21] Xiao P, Li Z, Zhu Z, Xiong X. Preparation, properties and application of C/C-SiC composites fabricated by warm compacted-in situ reaction. J Mater Sci Technol. 2010;26(3):283–8.
[22] Shi Q, Xiao P. Effect of pyrolytic carbon content on microstructure and tribological properties of C/C–SiC brake composites fabricated by isothermal chemical vapor infiltration. Solid State Sci. 2012;14(1):26–34.
[23] Akhtar M, Khajuria A. The synergistic effects among crystal orientations, creep parameters, local strain, macro–microdeformation, and polycrystals' hardness of boron alloyed P91 steels. Steel Res Int. 2022;93:2100819.